Bulletin of the Seismological Society of America, Vol. 109, No. 2, pp. 822–826, April 2019, doi: 10.1785/0120180250

Short Note

Interpretation of Kappa and f_{max} Filters as Source Effect

by Igor A. Beresnev

Abstract The high-frequency spectral rolloff of recorded ground acceleration during earthquakes is commonly modeled by either of the two *ad hoc* high-cut filters, f_{max} and kappa, which have been used interchangeably. The physical origin of the cutoff they produce is still debated, although it is more often attributed to the site effect. A natural extension of the earthquake source time function, radiating an omega-n spectrum into the far field, to noninteger n through the gamma function allows the spectral fall-off to be intermediate between the omega-square and omega-cube shapes, providing natural high-cut filtering exclusively as a source effect. The difference between applying the omega-2.5 source spectrum and the κ filter to simulate the high-frequency decay is no greater than the difference between applying the κ and its equivalent f_{max} filters. The conceptual advantage of employing the unfiltered omega-n source spectrum, with real $n > 1$, to represent the spectral decay of strong ground motions, is clear. This approach attributes the high-frequency behavior and its variability to a well-defined form of slip on an earthquake fault, making it unnecessary to introduce an artificial additional filter of unclear physical nature.

Introduction

A common model for the Fourier amplitude spectrum of the displacement pulse radiated into the far field by an earthquake source has the ω^2 (omega-square) dependence on frequency, in which the frequency-dependent term has the form:

$$D(\omega) = \left[1 + \left(\frac{\omega}{\omega_c}\right)^2\right]^{-1}, \quad (1)$$

in which ω is the angular frequency (Aki, 1967; Brune, 1970; Boore, 1983, 1986). Such a spectrum is flat at low ($\omega \ll \omega_c$) and decays as ω^{-2} at high ($\omega \gg \omega_c$) frequencies, in which ω_c is termed as corner frequency. The resulting ground-motion acceleration pulse has the amplitude spectrum $\omega^2 D(\omega)$, which grows as ω^2 at low and is flat at high frequencies.

Such a model nonetheless fails to describe a steep fall-off of the observed acceleration spectra beyond a certain high frequency termed f_{max} by Hanks (1982). This diminution is in addition to the decay produced by regular anelastic attenuation along the propagation path.

To describe the observed additional high-frequency suppression of the recorded spectra, two forms of *ad hoc* high-cut filters have been proposed, the one to use remaining a matter of choice. One is termed as f_{max} filter and the other as kappa filter. The former is described by the power frequency decay function

$$P(f) = \left[1 + \left(\frac{f}{f_{max}}\right)^8\right]^{-1/2}, \quad (2)$$

(Boore, 1983, his equation 4) and the latter by the exponential function

$$P(f) = e^{-\pi\kappa f}, \quad (3)$$

(Anderson and Hough, 1984, their equation 1), in which f_{max} and κ are the parameters. Both shapes (2) and (3) have been widely utilized.

The physical origin of the additional high-frequency filtering has been debated. For example, Hanks (1982) and Anderson and Hough (1984) considered it a characteristic of local site attenuation, whereas Papageorgiou and Aki (1983) attributed it to nonelastic material behavior at the tip of the propagating ruptures, that is, deemed it a source effect. Kilb *et al.* (2012) approached the existence of kappa as a combination of source and site effects, whereas Parolai (2018) linked it to the high-frequency trend of the transfer function of the medium due to wave propagation effects, such as refraction, reflection, and scattering. Weak correlations have been found between kappa and V_{S30} (the average shear-wave velocity in the upper 30 m of the geologic profile; Laurendeau *et al.*, 2013, p. 3132; Ktenidou *et al.*, 2015, their fig. 7). The main usage of the f_{max} and kappa filters is in strong-motion prediction based on the point-source model (Boore, 1983, 2003), but it should be remembered that the high-frequency slope is also modulated by the rupture directivity effects (Kaneko and Shearer, 2014a,b; Beresnev, 2017a, his equation 4 and p. 1279).

The goal of this study is to show that, within the realm of traditional applications, the ambiguity can be resolved by relaxing the requirement that earthquake spectra follow the commonly assumed omega-square shape, and by postulating their natural variability in deviation from the first negative power in equation (1). Indeed, it is hardly justifiable on physical grounds why nature necessarily favors the fault-slip functions that lead to the omega-square spectrum over other possible shapes. Once that restriction is removed, a possibility of steeper spectral fall-offs follows.

Theoretical Source Time Functions

Consider a slip on a fault described by an infinite functional series (source time function)

$$\Delta u_n(t) = U\left[1 - \frac{\Gamma(n+1, \frac{t}{\tau})}{\Gamma(n+1, 0)}\right], \qquad t \geq 0, \qquad (4)$$

in which $\Gamma(a, x)$ is the incomplete gamma function, $\Gamma(a, x) = \int_x^\infty e^{-t} t^{a-1} dt$ (Abramowitz and Stegun, 1964, their equation 6.5.3); the physical parameter τ describes how fast the fault dislocation rises to its final value U, and a is a real positive number (that is, the real $n > -1$ in equation 4). A useful relationship in the context of equation (4) is $\Gamma(n+1, 0) = \Gamma(n+1) = n!$, in which $\Gamma(a)$ is the gamma function (Abramowitz and Stegun, 1964, their equations 6.5.2, 6.5.3, 6.1.5).

The time derivative of the source time function defines the shape of the displacement pulse radiated into the far-field (Aki and Richards, 1980, their equation 4.32). The derivative of equation (4) is

$$\Delta \dot{u}_n(t) = \frac{U}{n!\tau}\left(\frac{t}{\tau}\right)^n e^{-\frac{t}{\tau}}, \qquad t \geq 0. \qquad (5)$$

The modulus of the Fourier spectrum of equation (5) (equation 5 is assumed to be zero at $t < 0$) is:

$$\Delta \dot{u}_n(\omega) = U\left[1 + \left(\frac{\omega}{\omega_c}\right)^2\right]^{-\frac{n+1}{2}}, \qquad (6)$$

in which we defined $\omega_c \equiv 1/\tau$. The frequency term in equation (6) becomes the exact omega-square spectral shape (1) for $n = 1$. The source time functions (4) thus produce the generic omega-n spectrum radiated into the far field, for any real $n > -1$. They provide a natural continuous extension of the spectral shapes into noninteger values of n. The forms of equation (4) in terms of elementary functions for integer $n = 0$, 1, 2 are provided by Beresnev and Atkinson (1997, their equations 5–7). For example, for $n = 0$, $\Delta u_0(t) = U(1 - e^{-t/\tau})$. Although formally equations (4) and (5) apply to all $n > -1$, the displacement pulse described by equation (5) is discontinuous at $t = 0$ for $n \leq 0$ and does not represent practical interest; we thus restrict our attention to the real positive values of n. The shapes of the functions (4) for $n = 1$, 1.5, 2 (radiating the omega-square, omega-2.5, and omega-cube spectra, respectively) in dimensionless form are plotted in Figure 1.

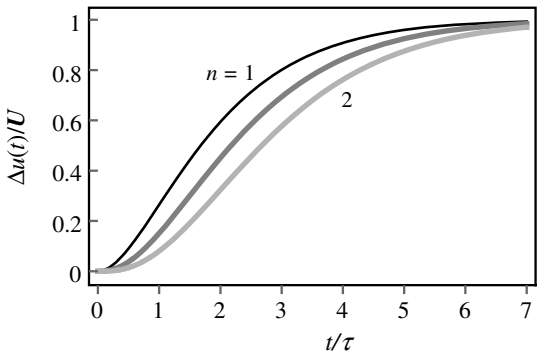

Figure 1. Source time functions (4) for $n = 1$, 1.5, 2.

Shapes other than the omega-square spectrum have been proposed (e.g., Boore, 2003, his table 2), but they are much less common.

The usage of the source time function in Kostrov's form

$$\Delta u(t) = \text{const}\ (v_r^2 t^2 - x^2)^{1/2}, \qquad t > \frac{x}{v_r}, \qquad (7)$$

in which v_r is the rupture propagation speed and x is the distance along rupture (Kostrov, 1964, his equations 3.5 and 4.9) can be encountered in the literature. The time derivative of equation (7) does not have a convergent Fourier spectrum, evaluated from $t > x/v_r$ to ∞; for this reason, the source time function (7) will not be considered further.

The physical nature of the formal parameter τ still needs to be clarified. The velocity of the slip (slip rate) on the fault is described by equation (5). By taking its derivative and equating it to zero, we find that the velocity reaches its maximum (denoted by $v_{\max}$) at the time $t = n\tau$. Substituting this time back into equation (5), we obtain

$$\tau = \frac{n^n}{n! e^n}\frac{U}{v_{\max}}, \qquad (8)$$

in which n is real positive. The two physical parameters U and $v_{\max}$ thus completely define the radiated omega-n spectrum (6).

Filtering Effect of the Omega-n Spectrum

The omega-n spectrum, for $n > 1$, provides natural high-cut filtering of the radiated acceleration spectra. It appears that an omega-cube spectrum ($n = 2$) is ruled out by the data (Boore, 1983, 1986). However, because it ensures steep high-frequency fall-off in its own right, a proper verification of the ability of the omega-cube model to reproduce strong-motion data would have to test it alone without applying the then-unnecessary *ad hoc* filters (2) or (3), which, to our knowledge, was not attempted. Setting this issue aside for the time being, we seek the value of n that lies between 1 and 2. Specifically, we will compare the filtering effect of

the spectrum with $n = 1.5$ with the effect of the f_{max} and kappa filters. No particular fitting of n was attempted; the value of 1.5 was chosen for purely aesthetic reasons; it corresponds to the middle curve in Figure 1.

There are two regional reference values of the parameter κ in equation (3) that are widely accepted in the literature. By fitting a large ground-motion database for western North America (WNA), Boore and Joyner (1997) deduced a generic value of $\kappa = 0.035$ s for an M_w 6.5 (M_w is the moment magnitude) earthquake on rock for that region. The frequency range of the data is 0.25–20 Hz (Boore and Joyner, 1997, their fig. 10). A lower value of $\kappa = 0.006$ s is generally accepted for eastern and central North America (ENA) (Toro *et al.*, 1997, p. 43). The frequency range is up to 20 Hz (Atkinson and Boore, 1995, p. 20).

It should be noted that the two high-frequency filters, equations (2) and (3), used in ground-motion prediction, are not identical, as they are described by two different functional forms—the power and exponential, respectively. As they are both commonly utilized, their approximate equivalence was proposed by Boore (1986, p. 58)

$$f_{max} \approx \frac{1}{\pi\kappa}. \tag{9}$$

Our comparison of the high-cut filtering effect of the f_{max} and kappa filters, on one hand, and the pure omega-2.5 source spectrum, on the other, is shown in Figure 2. To match the magnitude for which the generic WNA value of κ of Boore and Joyner (1997) was established, the comparisons are made for M_w 6 (the upper two panels, Fig. 2a,b) and M_w 7 (the lower two panels, Fig. 2c,d) earthquakes. As noted, two physical parameters are needed to define the omega-n spectrum (6): U and v_{max}, both of which enter the calculation of the corner frequency (8). The value of U was set from the respective magnitude by combining the definitions of the seismic moment $M_0 = \mu A U$ and the moment magnitude $M_w = (2/3)\log M_0 - 10.7$, in which μ is the shear modulus and A is the fault area. The shear modulus was obtained from $\mu = \beta^2\rho$ and $\beta = \alpha/\sqrt{3}$, in which α and β are the P- and S-wave velocities and ρ is the density. The values of α and ρ were taken as 5 km/s and 2700 kg/m^3, respectively. The fault area was set from the magnitude by the empirical relationship of Wells and Coppersmith (1994, their table 2A): $\log A = -3.49 + 0.91\,M_w$.

Based on seismological evidence, the velocities v_{max} are inferred to cluster in the range from about 0.2 to 2 m/s (Beresnev and Atkinson, 2002; Anil-Bayrak and Beresnev, 2009; Rowe and Griffith, 2015, their fig. 2). Two representative values were picked from this range, $v_{max} = 0.4$ and 1 m/s. Panels in Figure 2a,c are for 0.4 m/s and Figure 2b,d for 1 m/s.

The two gray lines on the top chart in each panel in Figure 2 present the omega-square acceleration spectra to which the κ filter was applied, with the two representative values of $\kappa = 0.035$ and 0.006 as indicated in the legend.

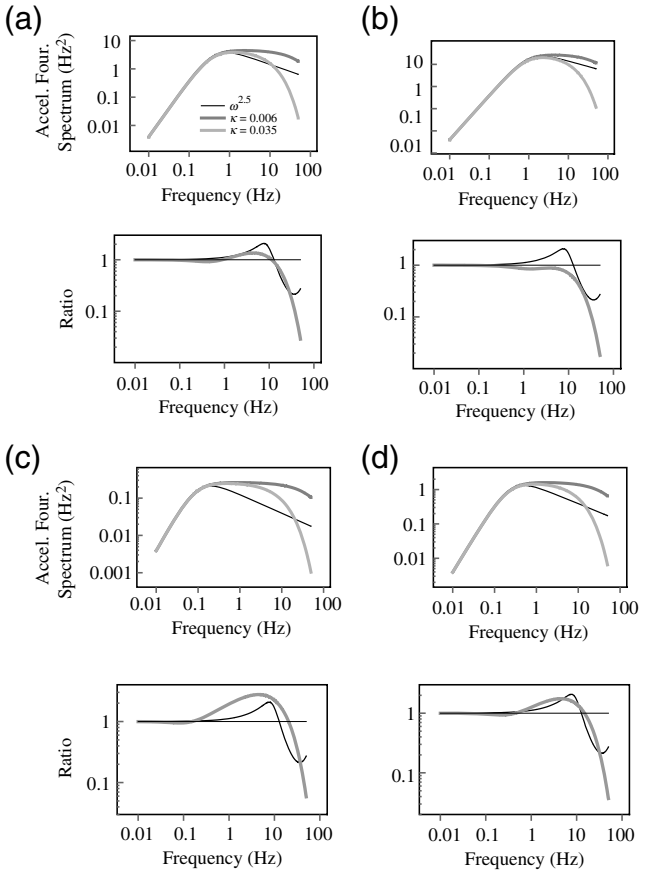

Figure 2. Comparison of the effects of the f_{max} and κ filters on the ω^2 spectrum with the filtering effect of the $\omega^{2.5}$ spectrum. (a, b) M_w 6, (c,d) M_w 7, (a,c) $v_{max} = 0.4$ m/s, (b,d) $v_{max} = 1$ m/s. Top charts in (a–d) show the ω^2 acceleration spectra to which the κ filter was applied (gray lines) and the unfiltered $\omega^{2.5}$ spectrum (black line). Bottom charts in (a–d) show the ratio of the f_{max} filter to its equivalent κ filter (black line) and the ratio of the κ-filtered ω^2 spectrum to the pure $\omega^{2.5}$ spectrum (gray line).

The spectra were computed for $n = 1$ as $\omega^2 \Delta\dot{u}_n(\omega) P(f)$, in which $\Delta\dot{u}_n(\omega)$ and $P(f)$ are defined by equations (6) and (3), respectively, and $\omega = 2\pi f$. The factor U in equation (6) was omitted in the calculation, giving the unit on the vertical axes of Hz^2. The corner frequency in each case was calculated from equation (8). The black line on the top chart in each panel is the unfiltered omega-2.5 acceleration spectrum calculated from equation (6) with $n = 1.5$ in the same manner but without $P(f)$ applied.

To evaluate the differences between the pure omega-2.5 and the filtered omega-square spectra on the top graphs in each panel, the ambiguity in choosing the particular type of the high-frequency filter, applied to the omega-square spectrum, should be taken into account. In the practical world of ground-motion simulations, it has often been a matter of choice whether to use the f_{max} or κ shapes to suppress the high frequencies. The black line on the bottom chart in each panel quantifies this ambiguity by presenting the ratio of the f_{max} filter (equation 2) to its equivalent κ filter (equation 3), for $\kappa = 0.035$ and its equivalent f_{max} determined from

equation (9). The gray line on the bottom charts is the ratio between the omega-square spectrum, to which the κ filter was applied, and the pure omega-2.5 spectrum (that is, the ratio of the light gray to the black lines in the respective top graph in the panel). In the bottom chart, the black line thus characterizes the general uncertainty arising from using the f_{max} versus the κ filters, and the gray one illustrates the uncertainty stemming from applying the κ filter versus the unfiltered omega-2.5 spectrum in WNA.

Discussion and Conclusions

Although the curves in Figure 2 were extended to 50 Hz on the horizontal axis, it should be remembered that the two representative values of κ used are strictly valid to 20 Hz only. The inspection of the bottom charts in each panel in Figure 2 shows that the black and the gray lines are no different in the magnitude of their deviation from one, on average, to the frequency of 20 Hz. This means that representing the κ-filtered omega-square spectrum by the unfiltered omega-2.5 spectrum is no more uncertain than using the omega-square spectrum filtered in two different but still acceptable ways. In other words, using the omega-2.5 spectrum, as the source effect, is equally plausible in simulating the strong ground motions as invoking a formal frequency filter with unclear physical origin. The conceptual advantage of the former approach is clear: it attributes the high-frequency rolloff of the ground motions to a well-defined form of slip on the earthquake fault (equation 4), rather than introducing the high-frequency decay in an artificial manner in the form of an *ad hoc* filter.

According to equation (8), for given n and v_{max}, the corner frequency increases with decreasing magnitude (the parameter U), which explains the relatively higher level of the omega-2.5 spectrum for M_w 6 (Fig. 2a,b) versus M_w 7 (the respective plots in Fig. 2c,d). This effect appears as if κ decreased with decreasing magnitude. The values of κ for western ($\kappa = 0.035$ s) and eastern/central ($\kappa = 0.006$ s) North America are distinctly different. At the same time, the observational base used to determine this parameter for ENA is notoriously lacking data in the large magnitude range. The dependence of κ on magnitude still remains an open question (Boore, 2003, p. 650).

In reality, the parameter n in the specific form of the fault dislocation rise (4) can be variable. There is no reason to believe that nature favors a particular value from the available continuum, within certain limits. In the respective κ (or f_{max}) space, this variability corresponds to the cloud of data points that can be fit with a region-specific value of κ only provisionally, with large ambiguity (Boore and Joyner, 1997, their fig. 10). For recordings of earthquakes at a given station, the natural scatter in n for different events will map into the variability around the station-specific mean κ. It should also be remembered that factors such as rupture directivity, wave propagation through stacks of layers, and site transfer function may disturb the high-frequency slope as well, causing the variations in the fall-off among different stations recording the same event. Natural variability in v_{max} in model (4) further contributes to the uncertainty in the ground motion that can follow.

Bindi *et al.* (2019) recently reported that residuals in ground-motion prediction equations are reduced at high frequencies by allowing deviations in the source spectra from the omega-square form. We find this conclusion consonant with the results of our study.

There is also a purely theoretical advantage of using a source time function (4) with $n = 1.5$ (radiating the omega-2.5 spectrum) over that with $n = 1$ (the omega-square spectrum) in numerical simulations of ground-motion radiation. The function (4) with $n = 1$ has a discontinuous second derivative, corresponding to ground velocity in the far field and leading to a theoretically infinite acceleration at $t = 0$. This is a difficulty, causing, for example, slow convergence of integrals over the fault plane in the simulation of earthquake radiation through the representation theorem, which modelers have experienced (Anderson and Richards, 1975, p. 349; Beresnev, 2017b, p. 4024). With $n = 1.5$, the second derivative (ground velocity) is continuous and the discontinuity is moved to the third derivative (ground acceleration), whereas the acceleration itself at $t = 0$ is finite.

Data and Resources

No data were used in the article. All inferences were made through the analyses of the respective equations and literature sources as indicated.

Acknowledgments

The manuscript benefited from constructive comments by D. Bindi.

References

Abramowitz, M., and I. A. Stegun (Editors) (1964). *Handbook of Mathematical Functions*, National Bureau of Standards, Washington, D.C.

Aki, K. (1967). Scaling law of seismic spectrum, *J. Geophys. Res.* **72,** 1217–1231.

Aki, K., and P. G. Richards (1980). *Quantitative Seismology*, W. H. Freeman and Company, San Francisco, California.

Anderson, J. G., and S. Hough (1984). A model for the shape of the Fourier amplitude spectrum of acceleration at high frequencies, *Bull. Seismol. Soc. Am.* **74,** 1969–1993.

Anderson, J. G., and P. G. Richards (1975). Comparison of strong ground motion from several dislocation models, *Geophys. J. Roy. Astron. Soc.* **42,** 347–373.

Anil-Bayrak, N. A., and I. A. Beresnev (2009). Fault slip velocities inferred from the spectra of ground motions, *Bull. Seismol. Soc. Am.* **99,** 876–883.

Atkinson, G. M., and D. M. Boore (1995). Ground-motion relations for eastern North America, *Bull. Seismol. Soc. Am.* **85,** 17–30.

Beresnev, I. A. (2017a). Factors controlling high-frequency radiation from extended ruptures, *J. Seismol.* **21,** 1277–1284.

Beresnev, I. A. (2017b). Simulation of near-fault high-frequency ground motions from the representation theorem, *Pure Appl. Geophys.* **174,** 4021–4034.

Beresnev, I. A., and G. M. Atkinson (1997). Modeling finite-fault radiation from the ω^n spectrum, *Bull. Seismol. Soc. Am.* **93,** 67–84.

Beresnev, I. A., and G. M. Atkinson (2002). Source parameters of earthquakes in eastern and western North America based on finite-fault modeling, *Bull. Seismol. Soc. Am.* **92,** 695–710.

Bindi, D., M. Picozzi, D. Spallarossa, F. Cotton, and S. R. Kotha (2019). Impact of magnitude selection on aleatory variability associated with ground-motion prediction equations: Part II–analysis of the between-event distribution in central Italy, *Bull. Seismol. Soc. Am.* **109,** doi: 10.1785/0120180239.

Boore, D. M. (1983). Stochastic simulation of high-frequency ground motions based on seismological models of the radiated spectra, *Bull. Seismol. Soc. Am.* **73,** 1865–1894.

Boore, D. M. (1986). Short-period *P*- and *S*-wave radiation from large earthquakes: Implications for spectral scaling relations, *Bull. Seismol. Soc. Am.* **76,** 43–64.

Boore, D. M. (2003). Simulation of ground motion using the stochastic method, *Pure Appl. Geophys.* **160,** 635–676.

Boore, D. M., and W. B. Joyner (1997). Site amplifications for generic rock sites, *Bull. Seismol. Soc. Am.* **87,** 327–341.

Brune, J. N. (1970). Tectonic stress and the spectra of seismic shear waves from earthquakes, *J. Geophys. Res.* **75,** 4997–5009.

Hanks, T. C. (1982). $f_{\max}$, *Bull. Seismol. Soc. Am.* **72,** 1867–1879.

Kaneko, Y., and P. M. Shearer (2014a). Seismic source spectra and estimated stress drop derived from cohesive-zone models of circular subshear rupture, *Geophys. J. Int.* **197,** 1002–1015.

Kaneko, Y., and P. M. Shearer (2014b). Variability of seismic source spectra, estimated stress drop, and radiated energy, derived from cohesive-zone models of symmetrical and asymmetrical circular and elliptical ruptures, *J. Geophys. Res.* **120,** 1053–1079.

Kilb, D., G. Biasi, J. Anderson, J. Brune, Z. Peng, and F. L. Vernon (2012). A comparison of spectral parameter kappa from small and moderate earthquakes using southern California ANZA seismic network data, *Bull. Seismol. Soc. Am.* **102,** 284–300.

Kostrov, B. V. (1964). Selfsimilar problems of propagation of shear cracks, *Appl. Math. Mech.* **28,** 1077–1087.

Ktenidou, O.-J., N. A. Abrahamson, S. Drouet, and F. Cotton (2015). Understanding the physics of kappa (κ): Insights from a downhole array, *Geophys. J. Int.* **203,** 678–691.

Laurendeau, A., F. Cotton, O.-J. Ktenidou, L.-F. Bonilla, and F. Hollender (2013). Rock and stiff-soil site amplification: dependency on V_{S30} and kappa (κ_0), *Bull. Seismol. Soc. Am.* **103,** 3131–3148.

Papageorgiou, A. S., and K. Aki (1983). A specific barrier model for the quantitative description of inhomogeneous faulting and the prediction of strong ground motion. Part II. Applications of the model, *Bull. Seismol. Soc. Am.* **73,** 953–978.

Parolai, S. (2018). κ_0: Origin and usability, *Bull. Seismol. Soc. Am.* **108,** 3446–3456.

Rowe, C. D., and W. A. Griffith (2015). Do faults preserve a record of seismic slip: A second opinion, *J. Struct. Geol.* **78,** 1–26.

Toro, G. R., N. A. Abrahamson, and J. F. Schneider (1997). Model of strong ground motions from earthquakes in central and eastern North America: Best estimates and uncertainties, *Seismol. Res. Lett.* **68,** 41–57.

Wells, D. L., and K. J. Coppersmith (1994). New empirical relationships among magnitude, rupture length, rupture width, rupture area, and surface displacement, *Bull. Seismol. Soc. Am.* **84,** 974–1002.

Department of Geological and Atmospheric Sciences
Iowa State University
253 Science I, 2237 Osborn Drive
Ames, Iowa 50011-3212
beresnev@iastate.edu

Manuscript received 5 September 2018;
Published Online 29 January 2019